J Ther Eng, Vol. 9, No. 6, pp. 1585−1603, November, 2023

Journal of Thermal Engineering
Web page info: https://jten.yildiz.edu.tr
DOI: 10.18186/thermal.1401255

Journal of Thermal Engineering

Research Article

Numerical analysis on heat transfer, flow structure and exergy loss of combined truncated and circular ribs in a square duct

S. Mohamed ILLYAS[1,*], Kumaresan VELLAISAMY[2], A. MUTHUMANOKAR[1]

[1]Department of Mechanical Engineering, B S Abdur Rahman Crescent Institute of Science and Technology, Chennai, 600048, India
[2]Department of Mechanical Engineering, Anna University, Chennai, 600025, India

ARTICLE INFO

Article history
Received: 07 May 2022
Revised: 17 January 2023
Accepted: 23 January 2023

Keywords:
Computational Fluid Dynamics; Heat Transfer; Ribbed Cooling; Exergy Loss; Nusselt Number; Friction Factor

ABSTRACT

The heat transfer, friction and exergy loss of a square duct with combined circular and truncated rectangular ribs are analyzed using computational fluid dynamics. The study is focused on the effect of rib arrangements on the flow and heat transfer performance. The analysis is carried out with six truncated rib angles varying between 15° and 90° and Re range of 12000 – 43000. The heat transfer is maximum in the middle part of the duct for 30° and 45° rib angles along span wise direction. The position of wake region is highly dependent on separation point over the circular rib as wake moves away radially from the axis of the duct for rib angles of 60°, 75° and 90°. The turbulent flow structures in large scale originates from side wall have marked effect on the heat transfer for the rib angles of 60°, 75° and 90° and with nearly with equal intensity for 15°, 30° and 45° rib angles. The exergy loss associated with friction is higher for 60° rib angle. While the normalized friction factor obtained with Fanning's equation varied between 1.8 and 4.2 and thermal hydraulic performance varied between 0.2 and 1.3 for the range of reexamined.

Cite this article as: Illyas SM, Vellaisamy K, Muthumanokar A. Numerical analysis on heat transfer, flow structure and exergy loss of combined truncated and circular ribs in a square duct. J Ther Eng 2023;9(6):1585−1603.

INTRODUCTION

Turbulators are being used to enhance the heat transfer performance of coolant in the channels. An increase in the demand for higher efficiency of gas turbines requires elevated gas inlet temperature which subsequently necessitates effective cooling of turbine blades. In order to withstand such an extreme thermal load on the blades an effective internal cooling technique needs to be developed. Internal cooling methods predominate the external cooling as it avoids the blending of gas and air enhancing the aerodynamic performance of the turbines. The commonly used internal cooling methods for turbine blades are jet impingement, rib turbulators and pin fins. Experimental and numerical studies have been performed to investigate the heat transfer performance of rib turbulators. An experimental study by Chandra et al. [1] examined heat transfer and friction behavior in a flow channel

***Corresponding author.**
*E-mail address: illyasmech4@gmail.com

This paper was recommended for publication in revised form by Regional Editor Md Hasanuzzaman

with a varying number of transverse ribs. They reported that the thermal performance associated with friction increases with number of ribs and developed the correlations to predict the heat transfer and friction factor as a function of Re and aspect ratio. Gao and Sunden [2] employed PIV technique to present the flow characteristics of the rectangular channel provided with staggered, inline and cross ribs. The results showed the strong effect of inclined ribs on the flow behavior in the development of secondary flows. Lu and Jiang [3] performed experimental and numerical investigations on a flow channel containing angled rib turbulators. The authors reported that the SST k-ω turbulence model is superior in the prediction of turbulent heat transfer over the RNG k-ε model. Chang et al. [4] examined a rectangular channel with V-shaped ribs on its performance indexed by (HTE) heat transfer enhancement ratio (Nu_{avg}/Nu_{∞}) for forward and backward flows (Re = 1000-30000). They obtained the Nu_{avg}/Nu_{∞} ratio = 6.8 for forward flows at Re = 30000 which they claimed that the highest among the available heat transfer enhancement (HTE) devices. Choudhury and Das [5] studied the viscoelastic effect of hydrodynamic flow over a porous plate. They derived approximate velocity, temperature fields and rate of heat transfer using perturbation technique. Choi et al. [6] presented a compound cooling technique with dimple and angled ribs on rectangular channels. The experimental results provided insight into the role of rib-induced secondary flow in the local Nu distribution. Mohammed et al. [7] investigated heat transfer and flow characteristics of vertical duct using nanofluids inducing mixed convection. They reported decrease in skin fiction coefficient with increase in Re and Pr. Xie et al. [8] carried out a numerical study on heat and transfer flow characteristics of a square duct with mid truncated ribs with varying angular positions for the Re range of 10000 – 50000. They reported that the presence of truncated rib develops secondary flow causing intense magnitudes of stream wise vorticity over the channel corner. Their results revealed that reduction in recirculating flow and the presence of large-scale stream-wise velocities enhances heat transfer. They concluded that 135° mid truncated rib provides higher heat transfer and 90° rib position offers relatively less pressure drop. An experimental study by Yaghmourali et al. [9] developed a thermal calorimetric flow meter with suspended cantilever structure. They reported presence of convection effect on the both sides of the active area due to suspended structure and lower velocity boundary layer thickness of the cantilever which enhances the sensitivity of the sensor. Singh et al. [10] compared the inline and staggered cross pattern ribs on their heat transfer and fluid flow characteristics (Re = 30000 - 60000). They reported that the rib-induced secondary flows increased the near-wall shear stress directly, which improved heat transfer on the end walls with rib turbulators. However, the staggered and inline pattern induce an increase in near-wall shear stress and the nature of the turbulence mixing caused by the two counter-rotating vortex pairs was different. Their study reveals that heat transfer enhancement of inline and staggered configurations are however similar the friction factor of inline arrangement is relatively lower. Wang et al. [11] numerically investigated heat transfer and flow characteristics of the wavy rib by varying the geometric parameters. They reported that rib height, radius and angle have a greater influence on heat transfer and flow structure while rib thickness is having little influence. Heat transfer performance and pressure consequences are positively correlated with rib height and angle while it is negatively correlated with radius. Numerical studies on heat transfer enhancement [12-15] with trapezoidal and cylindrical duct configurations were also carried out. The study investigated the thermo physical properties and thermal performance of nanofluids. Bahiraei et al. [16, 17] employed nanofluids for the exergy and entropy generation analysis in the study related to solar thermal applications and heat transfer enhancement techniques. Jing et al. [18] performed a numerical study on trapezoidal channel with slot and dimples. They analyzed the effect of dimple arrangement, rotation number (0 - 0.8) and channel orientation (0°- 60°) on flow and heat transfer characteristics under stationary and rotating states of the channel. They reported that rotation number has stronger influence compared to channel orientation on heat and flow characteristics and 108% improvement in Nu is achieved by increasing the rotation number. Heat transfer augmentation studies [19-21] were performed on the heat transfer devices using nanofluids. Bahiraei and Mazaheri [22] investigated the hydrothermal and irreversibility characteristics of grapheme based nanofluid with spiral heat sink. They reported diminishing temperature gradient with higher particle concentration leading to smaller irreversibility. Lee and Shih [23] numerically analyzed the effect of heat load (3.2 – 582 kW/m^2) on flow and heat transfer in cooling duct with staggered array of pin fins. They reported density and velocity variation in the boundary layer development due to heat load variation. They concluded heat transfer-induced changes in the flow field were found to allow Nu to be nearly constant in the post-entrance region even though Re is decreasing along the duct and to significantly slow the rate at which row-averaged Nu increases along the duct in the entrance region. Wei et al. [24] carried out comprehensive review on heat transfer characteristics in the trailing region of gas turbines. They reviewed the heat transfer characteristics of cooling method by using pin fin, latticework duct, dimple/ protrusion and film cooling. They reported that the however pin fin enhances the heat transfer in the trialing edge, the latticework duct has relatively high heat transfer ability compared to pin fin duct. They concluded that the protrusions/ dimples can improve heat transfer with low pressure loss. However, the heat transfer performance is less than that of a latticework duct or a pin fin duct. The

dimple/protrusion should therefore be paired with another cooling system. Luo et al. [25] experimentally analyzed thermal-hydraulic performance of a two pass duct with delta winglet vortex generator for its varying aspect ratio (length/height) and attack angle (30° - 90°). They reported 24% increase in thermal-hydraulic performance of the duct fitted with turbulator compared with smooth duct. They obtained highest thermal-hydraulic performance with low pressure drop with turbulator fitted with aspect ratio of 2 and 45° attack angle. Kumar et al. [26-28] performed heat transfer and exergy analysis of solar air heating system coated with nano particles. Their comprehensive study compared the heat transfer performance smooth and rough absorber plate with grapheme nanoparticles coating. Bahiraei et al. [29] used a spiral rib in a triple tube heat exchanger to study the irreversibility characterisitics of nanofluids. They reported decrease in entropy generation and exergy destruction by the decrease in rib pitch ratio. The studies [30, 31] emphasized heat transfer enhancement using PCM and nanofluids. Al-Dulaimi et al. [32] analyzed the heat transfer characteristics of a square channel with a vortex generator of varying attack angle (0°, 30° and 45°), block ratio (0.1, 0.15 and 0.2) and aspect ratio (1,1.5 and 2). They reported that turbulence generated by the vortex generator increases the heat transfer with an increase in block ratio. The larger aspect ratio causes the mixed flow region to move further down from the vortex generator resulting in reduced heat transfer. Their results revealed that the increase in attack angle until 35° increases the friction factor due to the formation of streamline flow over the vortex generator. The EARSM model is intermediate formulation between EVM and Reynolds stress (RSM) models in which RSM transport equations are reduced to algebraic form under equilibrium conditions. These models simply call for the solution of two transport equations and naturally take the effects of anisotropy into consideration. Additionally, there exist extensions that permit the incorporation of rotation and curvature effects in a manner consistent with the EARSM formulation. Even for fine near-wall meshes, EARSM appear to be more robust than RSM, although no anisotropic model will ever be as robust as linear eddy viscosity models.

According to the earlier studies, the internal cooling of gas turbine blades can be divided into three primary sections: a leading edge, a middle region and a trailing edge. While the jet impingement cooling is applied on the leading edge as stagnation flow by impinging jet can remove high heat load, the pin fin cooling is preferred for trialing edge. The middle region is primarily cooled by ribbed channels. Rib turbulators are always positioned on the interior surfaces of the blades in this area, on both the trailing and leading edges. In the case of rib turbulators the presence of ribs enhances heat transfer with redeveloping boundary layer following flow reattachment between the successive ribs. However the ribs increases the pressure drop in the flow stream. Therefore it is important to precisely predict the heat transfer associated with the friction characteristics. Most of the studies [1, 2, 3, 8, 10, 11, 23, 25, 32] address on heat transfer and pressure drop characteristics on rib or dimple alone flow channels. Besides the upstream flow condition potentially affecting the development of jet and heat transfer, the underlying physics involved in the flow structure has not yet been addressed in the earlier literatures. This necessitates a comprehensive analysis of flow structure. The current study focuses on the unique heat transfer augmentation features on the combination of two enhancement techniques with the provision of rectangular and circular ribs on the flow channel. The comprehensive study on flow structure involves vorticity, velocity fields, streamline and turbulence intensity. The application of the present study can be used for heat transfer enhancement in compact heat exchangers, micro heat exchangers used in electronic cooling applications, solar collectors and cooling of gas turbine blades. The objective of the present work is given as follows.

- To study the heat transfer and flow characteristics of truncated ribs of orientation varying between 15°- 90° and circular ribs placed centrally over a square duct.
- To analyze the friction factor and associated exergy loss of combined truncated and circular ribs for the Re range of 12000 and 43000.

PHYSICAL AND COMPUTATIONAL MODELS

The middle part of the turbine blade is generally cooled by internal ribbed passages. To simplify the computation, a ribbed flow channel with a square section is employed to simulate the mid part of the turbine blade passage with internal ribs. The height and width of the ribbed duct are 40 mm with a length of 500 mm. Truncated rectangular and circular ribs are provided on the flow passage as shown in Figure 1.The physical parameters considered for the duct and the rib are based on the studies conducted by Xie et al. [8] and Xie et al. [33] and Wang and Sunden [34] as shown in Table 1. The nomenclature of the flow channel and the rib are shown in Figure 2.The pitch distance selected for the truncated rib is 13% of the duct length Xie et al. [33] and the pitch distance for the circular rib is half of the pitch distance of the truncated rib. The length of the rib is selected considering the reattachment length varied between 4 to 7 times of the rib height Xie et al. [33].The rib height to hydraulic diameter ratio is (h/D_h) is fixed as 0.125 according to Wang and Sunden [34]. In the present study, a three-dimensional steady system is developed for a flow channel with a rib turbulator thereby focusing on flow dynamics and heat transfer intended to describe the effect of ribs on the flow field. Numerical analysis is performed using CFX. The simulation is performed based on the governing equations of fluid flow namely continuity, momentum and energy equations plus appropriate turbulence model as a closure. The flow channel consists of

three sections. The middle section consist of ribs arrangement and is provided with a heat source. The front and rear sections are provided with no ribs to obtain steady and fully developed flow to ensure computational accuracy. The geometric configurations of the flow channel are shown in Figure 1. The fluid is considered as air and supplied at a temperature of 303 K. The inlet boundary condition is provided with uniform velocity corresponding to the Re. The outlet condition is assigned with an average pressure of 1 bar. The bottom surface and confined surfaces (top and side walls) are provided with constant heat flux and adiabatic wall boundary conditions respectively.

In the present study, the Reynolds Averaged Navier Stokes (RANS) computations were carried out which requires solving of time-averaged governing equations. The velocity field in this method is divided into mean velocity $\overline{U}_i(x)$ and fluctuating velocity $U'_i(x,t)$ so that $U'_i = 0$. The time-averaged Navier-Stokes equations contains Reynolds stress as an additional term. Also the time-averaged energy equation is having turbulent heat flux as an additional term. To close the system of equations, these additional terms must be modelled. The time averaged governing equations for mass, momentum, and energy conservation can be expressed as [35]

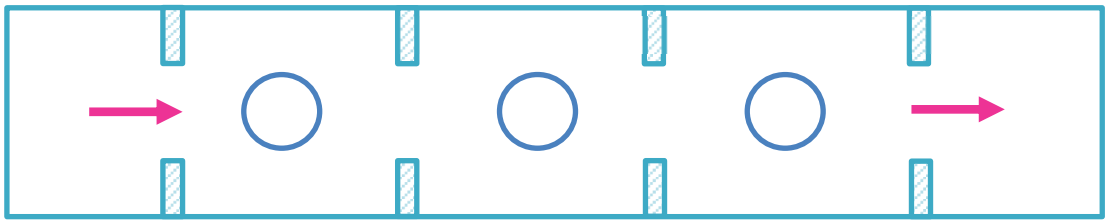

Figure 1. Physical model of the flow channel

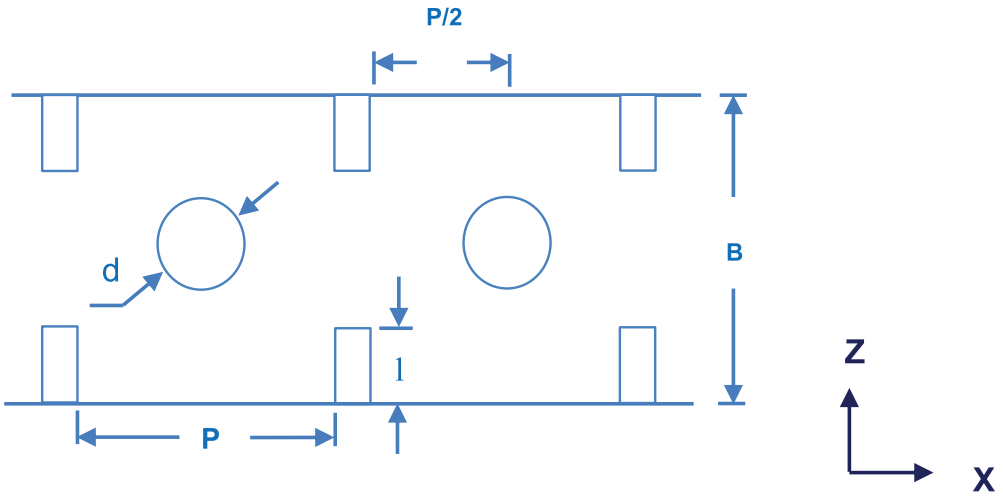

Figure 2. Nomenclature of the flow channel and ribs

Table 1. Geometric parameters of the ribbed duct

Geometric Parameter	Values, mm
Width of the duct, B	40
Height of the duct, H	40
Length of the duct, L	500
Height of the rectangular rib, h	5
Length of the rectangular rib, l	18
Diameter of circular rib, d	16
Pitch distance, P	70

$$\frac{\partial \rho}{\partial t} + \rho \frac{\partial U_i}{\partial x_i} = 0 \tag{1}$$

$$\frac{\partial \overline{U}_i}{\partial t} + \overline{U}_j \frac{\partial \overline{U}_i}{\partial x_j} = -\frac{1}{\rho}\frac{\partial \bar{P}}{\partial x_i} + \frac{1}{\rho}\frac{\partial}{\partial x_j}\left(\mu\left(\frac{\partial \overline{U}_i}{\partial x_j} + \frac{\partial \overline{U}_j}{\partial x_i}\right) - \rho \overline{U'}_i \overline{U'}_j\right) \tag{2}$$

$$\frac{\partial \bar{T}}{\partial t} + \overline{U}_j \frac{\partial \bar{T}}{\partial x_j} = \frac{1}{\rho}\frac{\partial}{\partial x_j}\left(\frac{\lambda}{c_p}\frac{\partial \bar{T}}{\partial x_j} - \rho \overline{U'}_i \overline{T'}\right) \tag{3}$$

Table 2. Turbulence models and other parameters in select numerical analysis on Ribbed duct

Literature	Re	Turbulators	Turbulence model
Wang et al. [36]	10000 - 40000	Wavy rib	SST *k-ω*
Singh et al. [10]	30000 - 60000	Angled Rib	SST
Wongcharee et al. [37]	3000 and 7000	Rectangular, triangular and cylindrical ribs	SST *k-ω*
Xie et al. [8]	10000 - 50000	Truncated rectangular rib	V^2 f
Liu and Wang [38]	10000 - 25000	Semi-attached rib	Reynolds Stress
Chaubo et al. [39]	3000 - 20000	Square ribbed wall duct	SST *k-ω*
Lin et al. [40]	25000	Cross ribbed duct	SST

The additional term in equation (2) is Reynolds stress tensor ($-\rho\overline{U'}_i\overline{U'}_j$) and in (3) is turbulent heat flux ($-\rho\overline{U'}_i\overline{T'}$).

In the present study, the eddy viscosity hypothesis is used to model the Reynolds stress as

$$-\rho\overline{U'}_i\overline{U'}_j = \mu_t\left(\frac{\partial\overline{U}_i}{\partial x_j}+\frac{\partial\overline{U}_j}{\partial x_i}\right)-\frac{1}{3}\rho\overline{U'}_i\overline{U'}_i\delta_{ij} \quad (4)$$

Where, μ_t denotes eddy viscosity and δ_{ij} refers to Kronecker delta, $\delta_{ij} = 1$ if $i = j$ and $\delta_{ij} = 0$ if $i \neq j$.

and turbulent heat flux is modeled as

$$-\rho\overline{U'}_i\overline{T'} = \frac{\mu_t}{Pr_t}\frac{\partial T}{\partial x_i} \quad (5)$$

Where, Pr_t is a turbulent Prandtl number.

SST *k*-ω model equation can be written as [41]

$$\frac{\partial}{\partial t}(\rho k)+\frac{\partial}{\partial x_i}(\rho k\overline{U}_i)=\frac{\partial}{\partial x_i}\left[\left(\mu+\frac{\mu_t}{\sigma_{k3}}\right)\frac{\partial k}{\partial x_i}\right]+P_k-\beta\rho k\omega \quad (6)$$

$$\frac{\partial}{\partial t}(\rho\omega)+\frac{\partial}{\partial x_i}(\rho\omega\overline{U}_i)=\frac{\partial}{\partial x_j}\left[\left(\mu+\frac{\mu_t}{\sigma_{\omega3}}\right)\frac{\partial\omega}{\partial x_j}\right]+(1-F'_1)2\rho\frac{1}{\sigma_{\omega2}\,\omega}\frac{\partial k}{\partial x_j}\frac{\partial\omega}{\partial x_j}+\sigma_3\frac{\omega}{k}P_k-\beta_3\rho\omega^2 \quad (7)$$

While *k*, ω, v, P_k denote the turbulent kinetic energy, turbulent frequency, kinematic viscosity and production rate of turbulence respectively whereas σ_3, β_3, $\sigma_{\omega2}$, $\sigma_{\omega3}$, σ_{k3} are model constants.

SST *k-ω* model over predicts the eddy viscosity as it does not include the transport of turbulent shear stress. A limiter to the formulation of eddy viscosity ensures the proper transport behavior as follows

Table 3. (a) Comparative results of Nu and friction factor for different turbulence models (b) Quantitative results for Nu distribution in Figure 4

(a)	***f/fo***	**% Deviation**	***Nu/Nuo***	**% Deviation**
Wang and Sunden [34]	2.950	---	2.152	---
RNG *k-ε*	2.189	-25.792	2.628	22.141
Reynolds stress	1.869	-36.652	2.543	18.189
k-ε	2.002	-32.127	2.623	21.877
k-ω	2.056	-30.317	2.552	18.597
SST *k-ω*	**2.110**	**-28.489**	**2.410**	**11.989**
BSL EARSM	2.082	-29.412	2.566	19.244
(b)	**Mean**	**Minimum**	**Median**	**Maximum**
Wang and Sunden [34]	2.152	1.760	2.180	2.400
RNG *k-ε*	2.628	2.508	2.615	2.751
Reynolds stress	2.543	2.263	2.449	2.952
k-ε	2.623	2.413	2.630	2.701
k-ω	2.552	2.267	2.463	2.958
SST *k-ω*	**2.335**	**2.078**	**2.284**	**2.679**
BSL EARSM	2.566	2.280	2.484	2.964

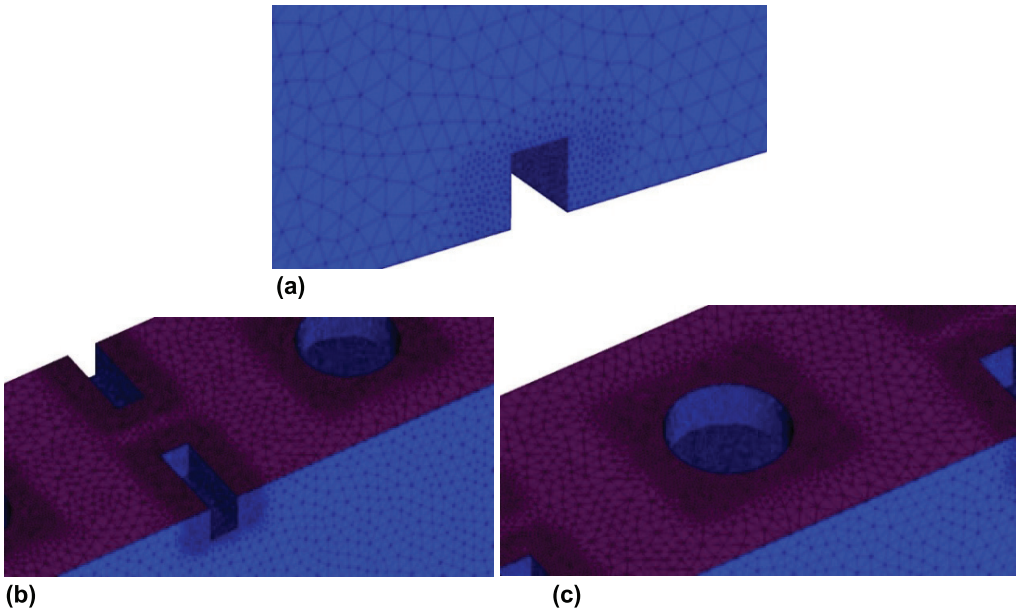

Figure. 3 (a), (b) and (c) Computational grid showing fine mesh near the truncated and circular ribs for 90° rib angle.

$$\nu_t = \frac{c_1 k}{\max(c_1 \omega,\ SF_2)} \tag{8}$$

$$\text{where } \nu_t = \frac{\mu_t}{\rho} \tag{9}$$

where S denotes an invariant measure of strain rate, c_1= 0.31 and F'_1, F'_2 are blending functions.

The various turbulence models used in the literature are given in Table 2. The quantitative results of friction factor and Nu are compared with the experimental results in Table 3. The tetrahedron and prism elements are used for discretizing the computational domain. The meshing parameters used for discretization are given in Table 4. The regions around the rib are provided with fine grids to resolve high velocity gradients as shown in Figure 3. With second order high resolution, the advection term is discretized. As the second order discretization scheme is less reliable than the first order in terms of convergence, the solution is first obtained using a first order upwind discretization method to improve the convergence with a residual value of 10^{-6}. The blend factor is then incrementally increased from 0 to 1 using initial values from previous results to ensure a second order high resolution scheme with similar convergence criteria at the final step of the solution.

Table 4. Meshing Parameters

Parameter	Value
Global element scale factor	1.3
Aspect ratio	1.1
Fillet ratio	0.1
Number of layers	5
Skewness	0.3
Maximum prism angle	180°

Table 5. Average Nu variation for different grid factors at *Re* = 23000 for 45° rib angle

Grid factor	Grid Nodes Million	Average *Nu*	Deviation of Average *Nu* compared to F6 %
F1	1.82	63.241	2.419
F2	2.74	63.781	1.586
F3	3.86	64.013	1.228
F4	4.72	64.179	0.978
F5	5.91	64.471	0.522
F6	6.41	64.809	---

Grid Independence Study

The grid independence of the solution is validated by performing a study on grid density. This is carried out by successive refining of mesh from a baseline value of 1.82 Million to a fine mesh value of 6.41 Million. Figure 4 shows the variation of average Nu with increasing number of grid size. The variation decreases with increase in number of grid elements. The Table 5 gives average Nu values for the selected grid factor values and their deviation from the reference grid factor of F6. F5 has the smallest variance, indicating that increasing the grid elements beyond F6 will only have a minor impact on the results. Therefore, the grid factor F5 is used in the present analysis to balance the computational time and accuracy.

Selection of turbulence model

Figure 5 shows the turbulence model obtained in the present analysis comparing the deviation of Nu/Nu_o with those experimentally obtained by Wang and Sunden [34]. While standard k-ε and RNG k-ε models are not predicting the experimental values and Reynolds stress, k-ω and BSL EARSM models reasonably predict the experimental values with a relative error of 12.46%,12.97% and 13.82% respectively corresponding to the region $4.2< x/p < 11.3$.

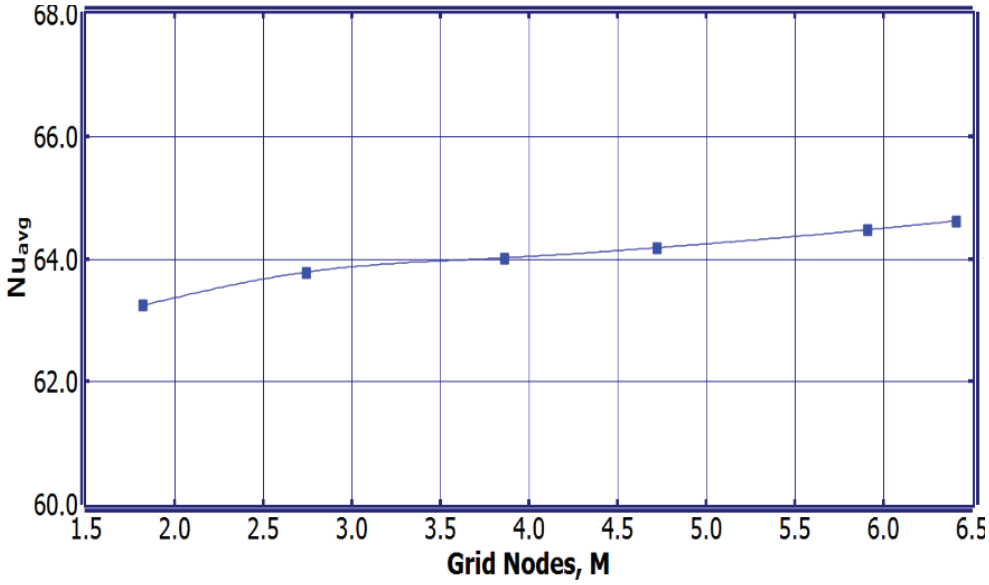

Figure 4. – Average Nu variation for different grid size

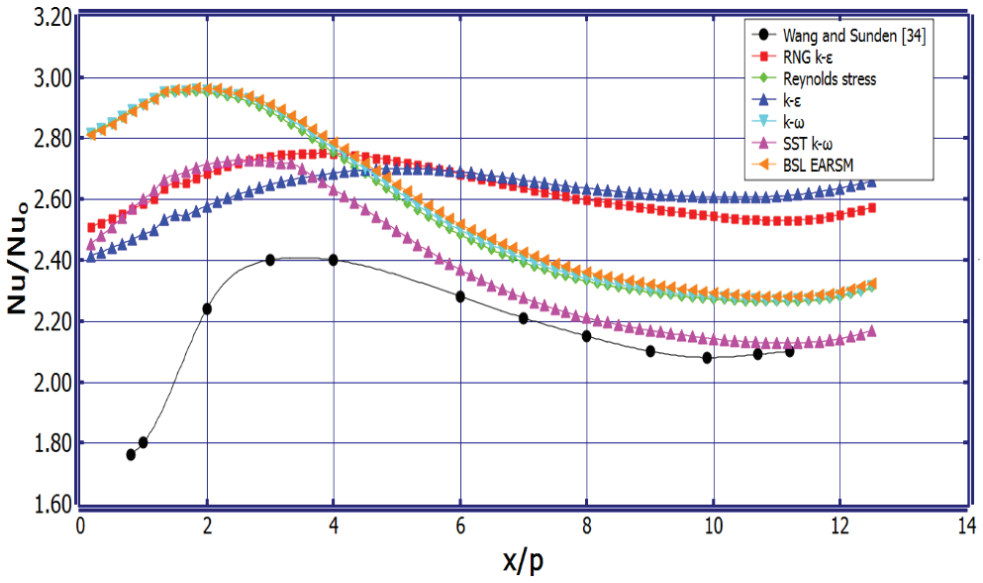

Figure 5. Nu number distribution for various turbulence models at Re = 12000 for 45° rib angle.

The SST *k-ω* model predicts relatively well in this region with a relative error of 5.12% and moderately in the region $0 < x/P < 4.4$ compared to other models. Wang et al. [36] showed that the predictions of SST *k-ω* and *k-ω* models are nearly the same and in good agreement with experimental results particularly at higher Re. They reported for three Re (10000, 25000 and 40000) the difference between experimental and numerical values (Nu/Nu_o) is about 53%, 26%, 14% respectively. Table 3 presents the turbulence models used in the earlier studies. The Table 3 shows quantitative results of friction factor and

Nu variation for various turbulence models. The SST *k-ω* model performs well with *k-ω* and *k-ε* equations, where the SST is used for predicting the flow field close to the wall where the viscous sub layer exists changes to the *k-ω* for turbulent flow with a blending function providing smooth change between SST and *k-ω* models. As SST *k-ω* gives precise computations on separation of flow with pressure gradient [42] for flow fields containing rotation and recirculation [41], it is chosen in the current study.

Data Reduction

In the present study, the heat transfer and friction factor are considered to describe the performance of internal cooling of the channel with varying rib arrangements. The performance parameter associated with heat transfer is defined based on the Nu [43]

$$PF_{Nu=} \frac{1}{A}\int \frac{Nu}{Nu_0}\, dA \tag{10}$$

Where N_u is given by the equation [40, 43]

$$Nu = \frac{q\, D_h}{k_a\,(T_w - T_a)} \tag{11}$$

N_u is the local Nu obtained on the duct surface. While *A* is an area of the heated surface, T_w and T_a are the wall temperature and air temperature respectively. q is the heat flux imposed on the heated surface and k_a is the thermal conductivity of air.

The friction factor referring to pressure drop in dimensionless form with the presence of ribs is given by Fanning's definition [8]. The performance parameter relating to friction factor (*f*) due to pressure drop is defined as [43]

$$PF_f = \left[\frac{f}{f_0}\right]^{\frac{1}{3}} \tag{12}$$

Where *f* is given by the equation [43]

$$f = \frac{\Delta p\, D_h}{2\,\rho_a\, U_i\, L} \tag{13}$$

Where *ΔP, ρ, U_i and L* refer pressure drop, the density of air, mean velocity at inlet and duct length respectively.

Exergy balance for a steady system can be obtained by first and second laws of thermodynamics [44] in equations (14) and (15) respectively,

$$Q - W = \Delta H \tag{14}$$

$$Q = T_0\, \Delta S \tag{15}$$

Equations (14) and (15) give,

$$W = T_0\, \Delta S\ - \Delta H \tag{16}$$

Since the exergy is the maximum useful energy available from the system as it reaches a dead state [44]

$$\dot{E}_{out} = W_{max} = T_0\,(S_0 - S)\ - (H_0 - H) \tag{17}$$

The useful work in reversible process of steady flow system [44]

$$\dot{E}_{in} = \left(1 - \frac{T_0}{T}\right) Q \tag{18}$$

$$\dot{E}_{loss} = \dot{E}_{in} - \dot{E}_{out} \tag{19}$$

RESULTS AND DISCUSSION

Stream and Velocity Fields

The streamline flow along the duct for various rib angles is shown in Figure 6. It can be seen that the streamline for all the rib arrangements reveals the flow separation zones associated with rectangular and circular ribs. The secondary flow originates from the side wall just behind the rectangular ribs and moves inwards towards the center line of the duct as shown in Figure 6. The induced secondary flows enhance turbulence in the vicinity of the rib resulting in increased heat transfer as it is seen in Nu distribution in Figure8. It is seen that the symmetric flow pattern as well as recirculation zone appearing along the stream-wise direction for rib angles 15°, 30° and 45° (Figure 6 a, b, c) with increasing size of recirculation zone with increasing angle between 15° and 45° (Figure 6 a, c). The induced secondary flow due to symmetric larger recirculation zones has relatively significant interaction over the bulk flow with enhanced mixing causing a peak Nu in the span-wise direction for 30° and 45° as shown in Figure 6 b, c. While a larger recirculation zone appearing at the upper region behind the rectangular rib directs most of the flow stream to the lower part of the circular rib (towards the side wall) for the rib angle of 60° (Figure 6 d) whereas the flow stream is directed upper part of the circular rib due to

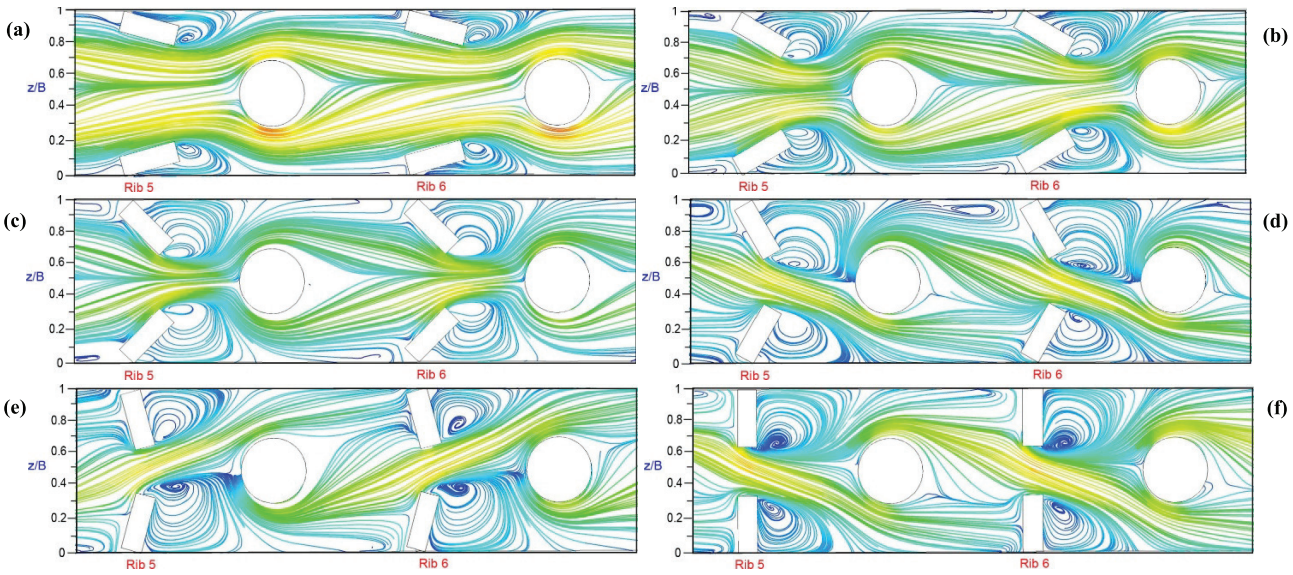

Figure 6. Flow streamlines along stream wise direction in the 5th and 6th row of ribs for rib angles 15° - 90° at Re = 12000. (a) 15° (b) 30° (c) 45° (d) 60° (e) 75° (f) 90°.

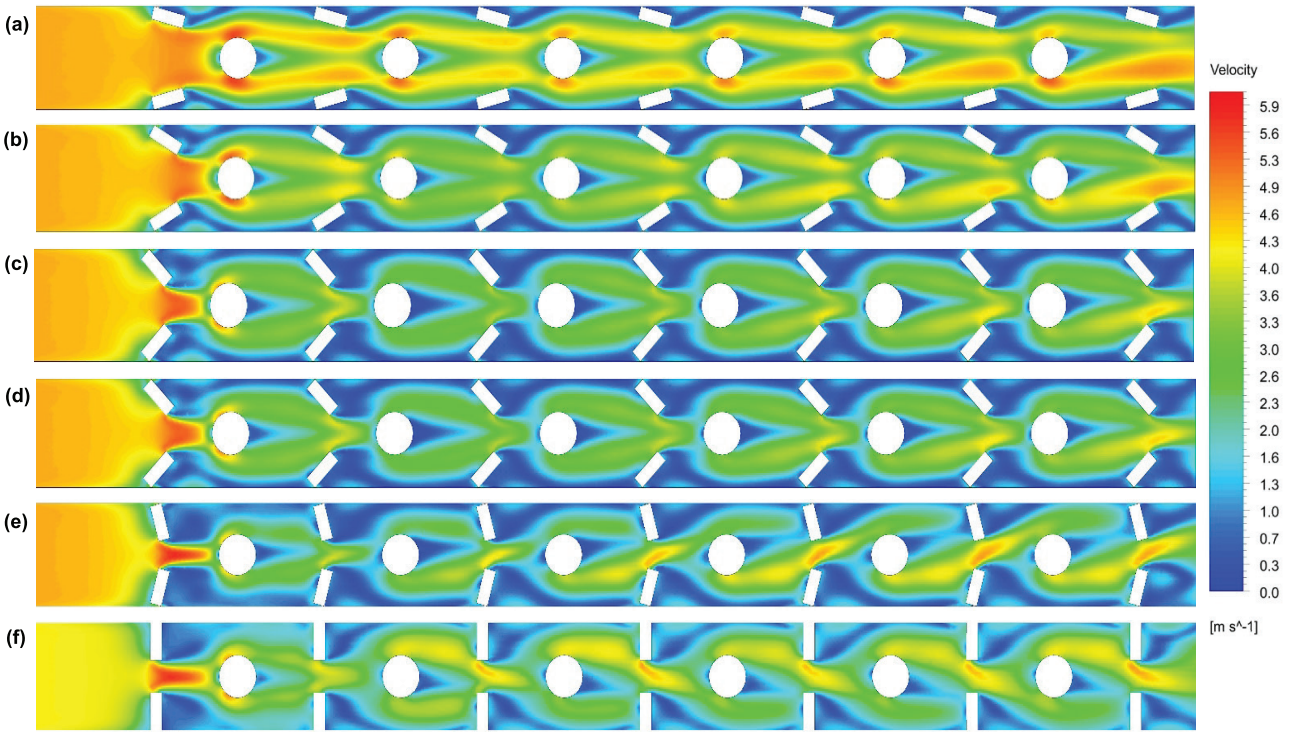

Figure 7. Velocity variation along streamwise direction for rib angles 15°- 90° at Re = 12000
(a) 15° (b) 30° (c) 45° (d) 60° (e) 75° (f) 90°.

a larger recirculation zone at the lower part behind the rib angle of 75° (Figure 6 e). On relative comparison of heat transfer enhancement in this region (side walls of the circular rib), it is seen that the Nu has significantly increased for the rib angle of 60° and 75° as shown in Figure 8 d, e compared with the other rib arrangements. Thus with the 60° and 75° rib arrangements the heat transfer rate is relatively better than other arrangements. The flow approaching the circular rib spreads out and moves around causing a boundary layer separation. On separation the wake is

formed in the separated flow region behind the circular rib as shown in Figure 6. It is observed that the position of the wake region is highly dependent on the separation point over the circular rib as the wake moves away radially from the axis of the duct for rib angles of 60°, 75° and 90° (Figure 6 d, e, f). The presence of the wake behind the circular rib causing turbulent eddy motion and vortex formation resulting in an increased heat transfer rate as higher Nu is observed as shown in Figure 7 for all cases. Figure 7 shows mean velocity variation for the various rib arrangements. The velocity field behind the rib near the wall reduces significantly with the presence of recirculation zones. This lower velocity zone seen as maximum for the 90° (Figure 7 f) rib angle implying a larger recirculation zone just past the rib. As the flow progressed further past the circular rib the nature of secondary flow induced at the side walls are different with those found for the rectangular rib as it is seen in stream line flow in the Figure6. As it is seen that the lower velocity field appears at the wake region and it intensifies for the rib angles of 60°, 75° and 90° (Figure 7 d, e, f) along the flow direction. While the flow separation is minimal at the lower part as observed in streamline flow in Figure6 between the rectangular and circular ribs resulting in increased velocity in that region for 15° and 30° (Figure 7 a, b) angles whereas 60°, 75° and 90° (Figure 7 d, e, f) cases exhibiting intense flow separation at the downstream of rectangular rib causing a reduced velocity field. When the fluid moves over the circular rib beyond the stagnation point it accelerates first over the front portion and decelerates as it passes round the rear portion due to an adverse pressure gradient resulting in flow reversal and separation as shown in Figure 7. It can be seen that the flow deceleration is relatively higher for 60° and 75° (Figure 7 e, f) rib arrangements resulting in the intense wake region.

Nu Field

Figure 8 shows the Nu distribution between Rib 5 and 6. While the overall heat transfer is low and a local peak appears at the rib area for 15° and 30° (Figure 8 a, b) whereas non-uniform heat transfer appears at either side of the rib for 75° and 90° (Figure 8 e, f) cases. The heat transfer has a marginal increase along the stream wise direction for the cases 15° and 30° (Figure 8 a, b) and the influence of rib at downstream is marginal. On contrary, the heat transfer increases as the high Nu area appears at downstream for the cases 45° and 60° (Figure 8 c, d). The enhanced heat transfer appears as the Nu increases along the flow direction for 45° (Figure 8 c). The lower heat transfer is observed in the region between the two consecutive ribs. This is fact is due to redeveloped boundary layer past the rib region. The flow separates and reattaches at the downstream of the rib forming a recirculating region also shown in Figure 5 resulting in increased Nu.

as shown in Figure 8 and its intensity is high for 45° and 60° (Figure 8 c, d) cases. The flow separation and reattachment are due to an adverse pressure gradient caused by the next rib as shown by Wang and Sunden [34]. The flow separation downstream of the rib causing a reduction in Nu

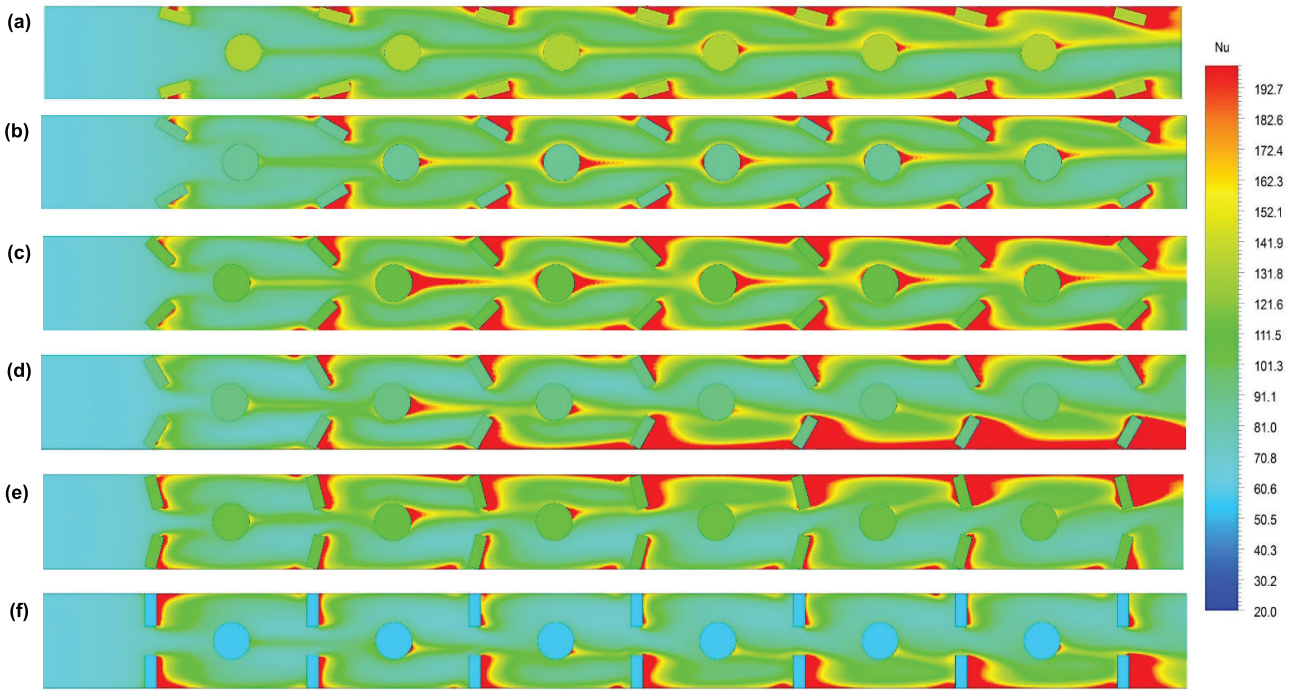

Figure 8. Nu number distribution along stream wise direction for rib angles 15°- 90° at Re = 12000

15° (b) 30° (c) 45° (d) 60° (e) 75° (f) 90°

exhibits symmetry about the flow axis for 15°, 30°, 45° and 90° cases (Figure 8 a, b, c and f).

Nu decreases and reaches its minimum in the middle part of the channel for 90° (Figure 9 f) and a marginal rise for 75° (Figure 9 e) rib arrangement. This shows that heat transfer augmentation is weakened in the middle part of the channel for 75° and 90° (Figure 9 e, f) rib angles. The lower Nu at the middle part than those observed near the side wall, probably due to intensified secondary flow at the side walls than at the middle region as observed by Wang and Sunden [34] in his study for a square duct with continuous ribs.

The Nu peak is relatively higher in the middle part of the duct for 15°, 30° and 45° (Figure 9 a, b, c) rib angles while this peak is not found in the other cases. The normalized Nu number variation along span-wise direction for various rib angle positions is shown in Figure 9 a, b. The Nu number has a peak in the center part of the duct along the span wise direction. The normalized Nu number increases along the span-wise direction at each *z/B* location towards the channel center line and reaches a maximum for the rib angles between 15° and 60° (Figure 9 a, d). The increase in Nu is attributed to the enhanced turbulence associated with decreased mean velocity along the spanwise direction. A trend analysis (second order polynomial) for the increase in normalized Nu number for 15° and 60° rib angles towards center line in span wise direction is shown in Figure 10. This further implies that turbulence behavior has strong influence on the heat transfer in span wise direction. Whereas this trend is contrary as the This increase in Nu

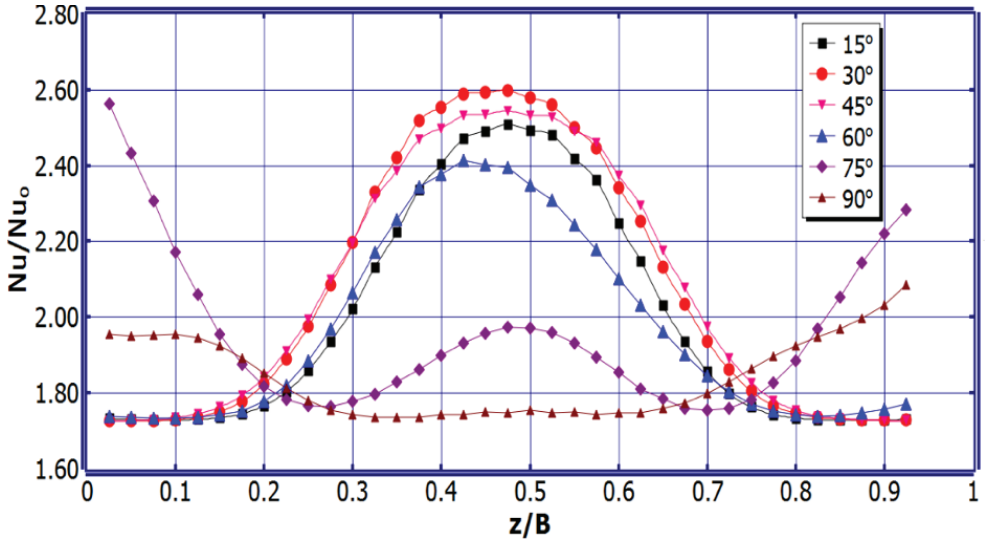

(a)

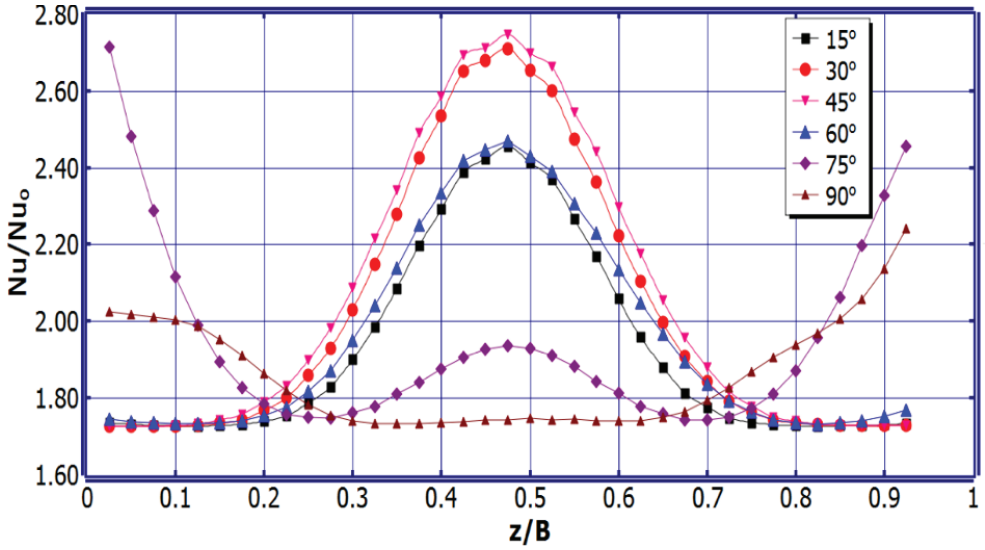

(b)

Figure 9. Nu variation along span wise direction at *Re* = 12000 (a) Upstream of 4th Rib (b) Downstream of 4th Rib

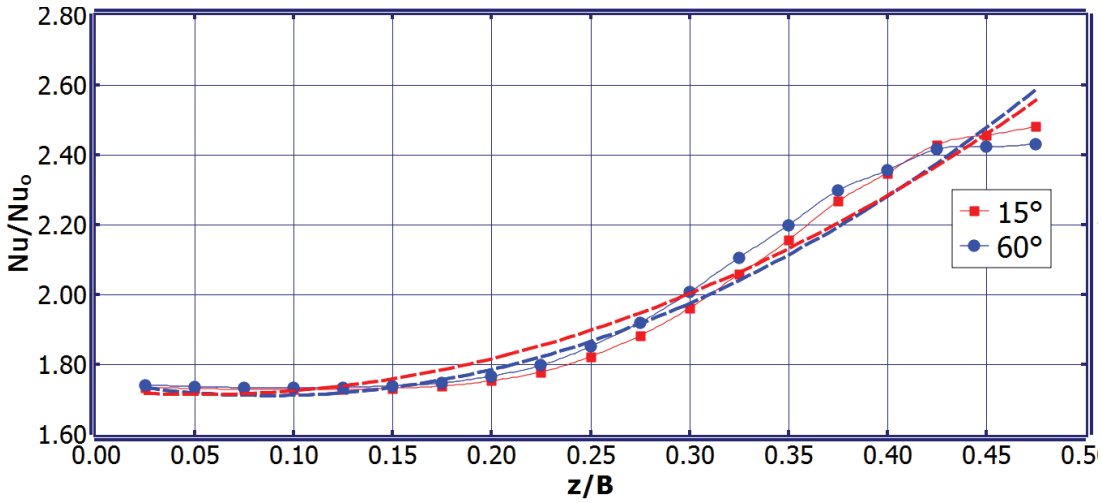

Figure 10. Polynomial trend analysis for the increase in Nu for 15° and 60° rib angles in spanwise direction.

is attributed to the presence of the wake region just behind the cylindrical rib as it is seen in streamline plot (Figure 6) where the high turbulence prevails. However, the Nu peak is marginally lowered the heat transfer uniformity has increased along spanwise direction for the rib angle of 60° as shown in Figure 9 d. As the flow progressed further past the truncated rib the resulting turbulent mixing with the interaction of bulk flow influences the heat transfer characteristics in the span wise direction as shown in Figure 9 b. As it is seen that the Nu distribution in the middle part of the duct is varying compared with those upstream of rectangular ribs (Figure 9 a). The Nu peak for the rib angle 30° and 45° at downstream of the rib (Figure 9 a) reaches their maxima compared to the rib upstream (Figure 8 b). This fact is due to the formation of symmetric secondary recirculation zones at near wall in the vicinity of the rib as observed in streamline (Figure 6) resulting in increased Nu. While the increase in Nu number is observed in the middle part of duct for the rib angles of 15°, 30°,45° and 60° as shown in Figure 9 b compared to the rib upstream (Figure 9 a) the variation is marginal for the rib angle of 75° and 90° positions. However the increase in Nu is significant at the side walls for 75° and 90° rib angles as shown in Figure 9b.

Vorticity and turbulence kinetic energy fields

Figure 11 shows the vorticity in the span wise direction. The existence of intense vorticity is apparent in the flow stream at the vicinity of the rib as well as side walls due to velocity gradients causing shear layer at jet edges. The development of such vortices towards the side wall of the duct which are coherent in nature for rib angle 15°, 30° and 45° (Figure 11 a, b, c) enhancing turbulence thereby increasing the heat transfer rate near the ribs. While relatively larger vortices on one side of the duct for the rib angle 60°, 75° and 90° (Figure 9 d, e, f) affecting the uniformity of vorticity distribution along span-wise direction as shown in Figure 11 e, d and f. The weak vortices are observed in the middle part of the duct spread out in the span wise direction for rib angle of 75° and 90° as shown in Figure 11 e, f. Whereas with increasing z/B distance from the middle of the duct the shear layer develops outward resulting in an increase in vorticity for rib angles 75° and 90° (Figure 11 e, f). On the other hand, the existence of two shear layers one in the inner and another in the outer region of the flow causes strong vortices and leaves behind a weak vorticity zone between these two regions for rib angles between 15°, 30° and 45° as shown in Figure 11 a, b, c. Figure 10 shows the intensity of turbulence for the various rib arrangements. It is seen that the turbulence originates from both corners of the side wall with nearly equal intensity and travels inwards towards the channel center line for 15°, 30° and 45° rib angles (Figure 12 a, b, c). The turbulent fluctuations are primarily due to the flow reversal causing the secondary vortices which developed behind the rectangular ribs. The secondary vortices formed in the shearing layer of flow may get through into the boundary layer and offer mixing of fluids of differing temperature as well as kinetic energy causing a local rise in heat transfer as they disperse downstream according to Zuckerman and Lior [45]. The turbulent flow structures in large scale as observed for the rib angles of 60°, 75° and 90° (Figure 12 d, e, f) originating from one side wall have marked effect on the heat transfer.

However they extend more towards on wall side for 75° and 90° (Figure 12 e, f) cases whereas the turbulence spreading is towards the center of the duct for 60° (Figure 12 d) rib angle and with nearly equal intensity for 15°, 30° and 45° (Figure 12 a, b, c) rib arrangements as reported earlier. This equal intensity of turbulent flow structure leads to uniform heat transfer towards the middle part of the duct.

Thermal performance and Exergy loss

Figure 13 shows the normalized Nu variation for the Re range between 12000 and 43000. Nu decreases gradually with an increase in Re which is consistent with the results

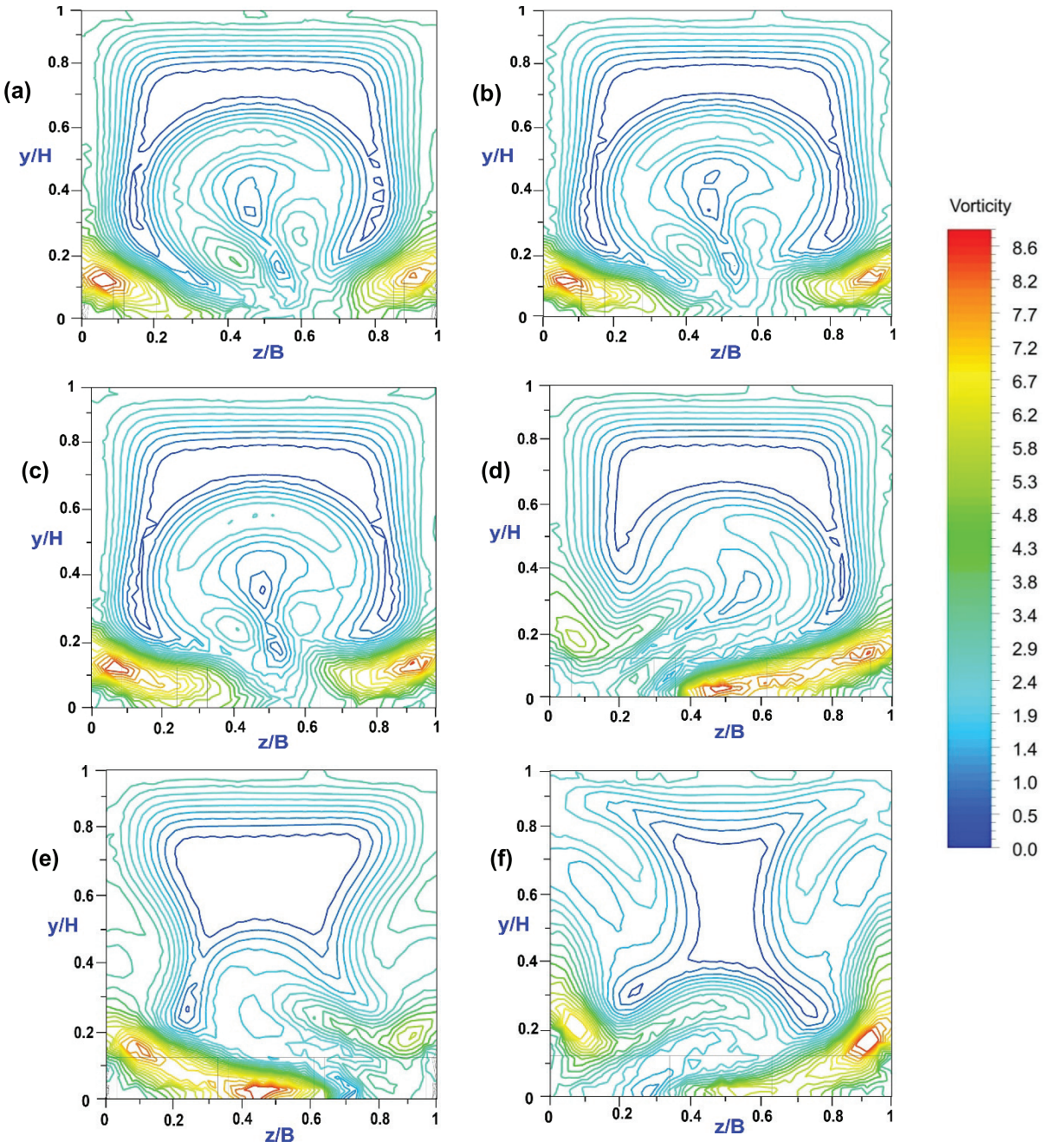

Figure 11. Vorticity distribution ($\omega D_h/U$) along spanwise direction for rib angles 15°- 90° at Re = 12000

(a) 15° (b) 30° (c) 45° (d) 60° (e) 75° (f) 90°

of Wang and Sunden [34] and Tanda [46]. It can be seen that the Nu is relatively higher for 60° rib angle showing heat transfer enhancement at lower Re followed by 75° position. The Nu for 30° rib angle is marginally lower than 15° and 45° rib positions at lower Re. Figure 14 shows the normalized friction factor (f/f_0) for the various rib angles. However higher heat transfer obtained from turbulence enhancement

usually causes a higher pressure drop, the (f/f_0) trend is different from the normalized Nu distribution. While 15° rib angle shows relatively lower pressure drop at all ranges of Re, the 90° rib arrangement exhibits a higher pressure drop. Though the pressure drop for the 75° rib position is lower than the 90° rib position at a lower range of Re number its magnitude reaches close to the 90°. While the thermal-hydraulic performance shown in Figure15 is relatively lower for the 90° rib angle, it is higher for the 60° case at a lower Re and marginally reduces with increasing in Re compared with the 15° arrangement. The exergy losses represent difference between the maximum available energy

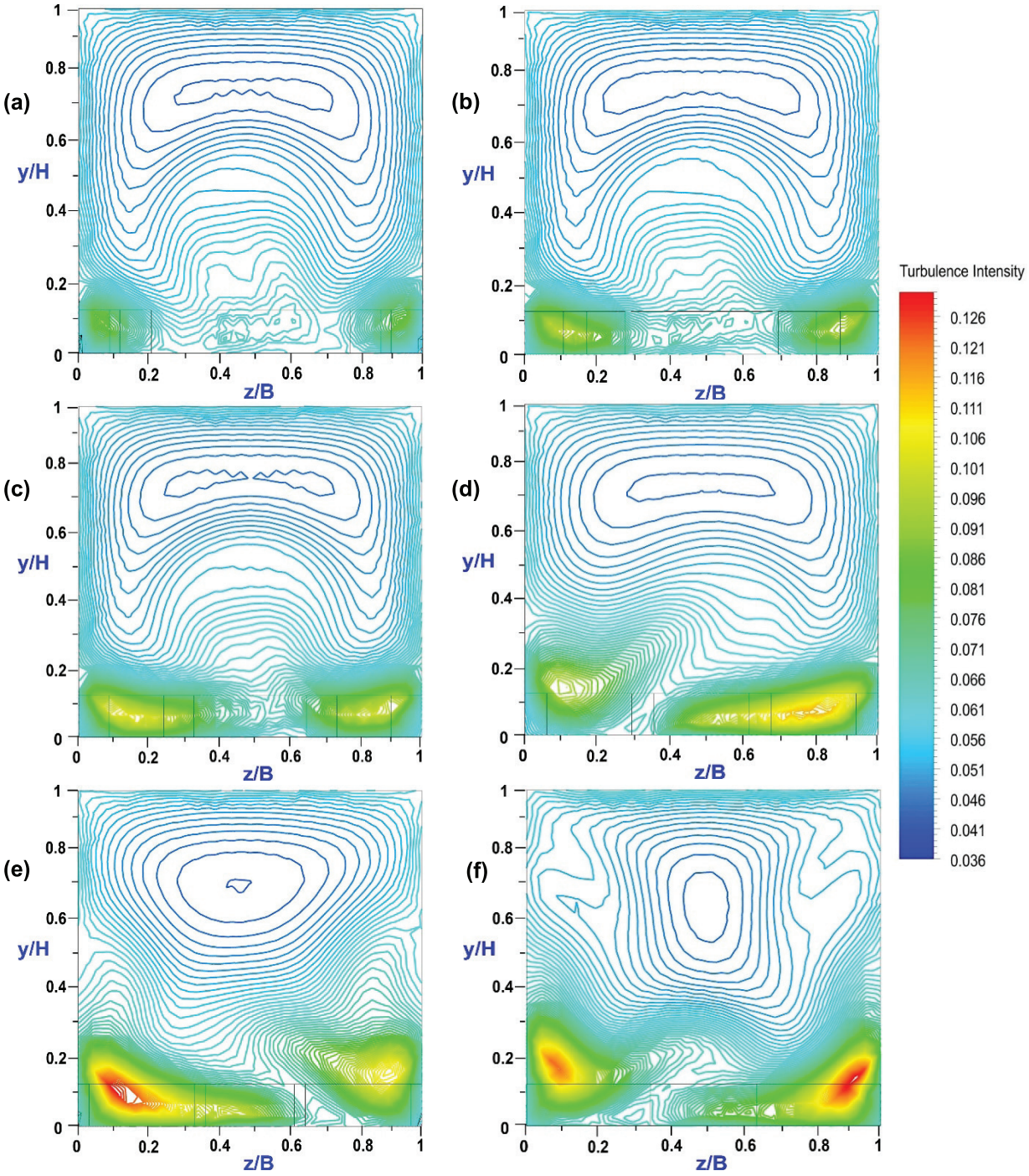

Figure 12. Intensity of turbulence along span wise direction for rib angles 15°- 90° at Re = 12000
(a) 15° (b) 30° (c) 45° (d) 60° (e) 75° (f) 90°

and actual energy. The exergy loss for varying Re and rib angles are shown in Figure 16. The trend shows that exergy loss increases with increases in Re which is an agreement with studies of Elwekeel et al. [47] and Kottayat et al. [48]. The exergy loss for 60° rib angle is relatively higher compared with other rib angles and followed by 75° rib arrangement. The increase in exergy loss for the 60° and 75° angles is 51.3% and 46.1% respectively when the Re is increased from 23000 to 33000 and it is 47.1% and 45.6% respectively when it is increased from 33000 to 43000. The exergy loss is maximum for the 60° rib arrangement for the Re of 23000, 33000 and 43000. The average heat transfer rate is relatively higher in the case of 60° rib angle as observed in Figure 7 which incurs more exergy loss compared to other rib angles.

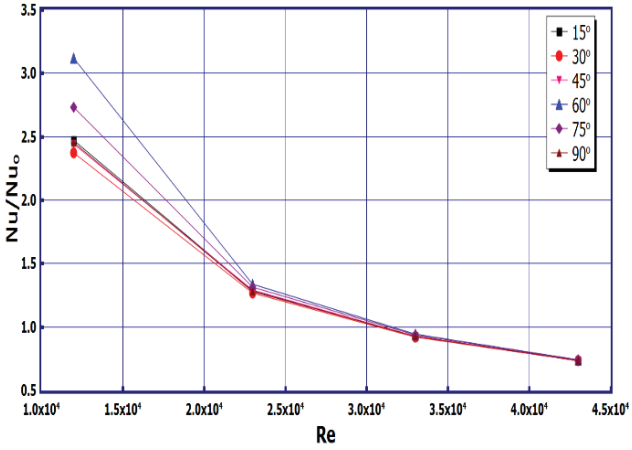

Figure 13. Normalized Nu for rib angles of 15°- 90° at *Re* = 12000 - 43000

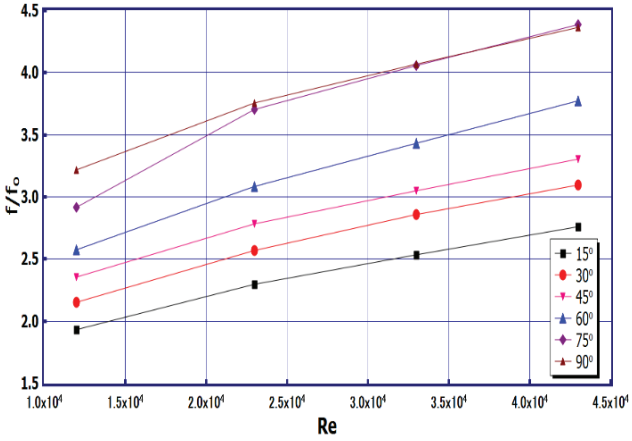

Figure 14. Normalized friction factor for rib angles of 15°- 90° at *Re* = 12000 - 43000

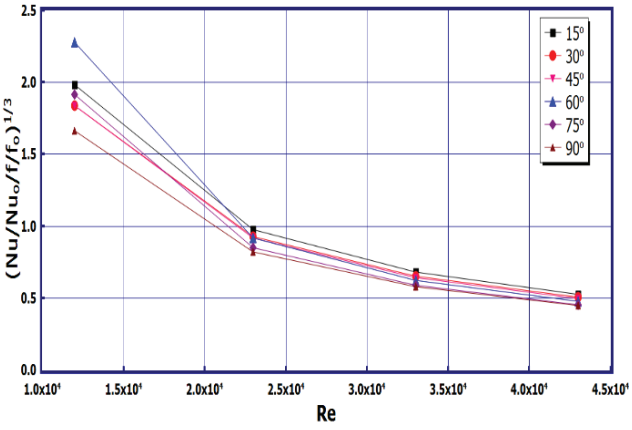

Figure 15. Thermal hydralulic performance for rib angles of 15°- 90° at *Re* = 12000 – 43000.

Comparison with Previous Studies

The present average Nu ratio (Nu/Nu_0) for the rib angles of 15° - 90° is compared in Figure 17 a with the average friction factor ratio (f/f_0). The highest Nu enhancement is given by 60° continuous ribs and delta backward ribs employed by Han and Park [49] and Han et al. [51].

It is observed that the magnitudes of such enhancement are significantly influenced when a particular rib configuration is provided with varying rib height, pitch, relative spacing and blockage. The results for 30° and 60° rib angles are reasonable with the results of Han and Park [49] and the 90° rib angle is comparable with Han and Park [49] and Han et al. [50]. The performance factor $Nu/Nu_0/f/f_0$ as it varies with f/f_o are compared in Figure 17 b. The values of $Nu/Nu_0/f/f_0$ are varying between 0.68 – 1.1 for the rib angles of 15° - 90°. As such the present values show reasonable performance relative to previous studies [48-50]. The scatter plot of showing the deviation is shown in Figure 18.

CONCLUSIONS AND RECOMMENDATIONS

The heat transfer and flow characteristics of ribbed wall duct were numerically studied. The results were predicted with SST *k-ω* turbulence model with Re number varying between 12000 and 43000. The important conclusions of the present study are as follows:

- The key findings on the flow field reveal that the turbulent flow structures in large scale developed on the wall side enhance the uniformity of Nu distribution with reduced magnitude for 60° rib angle. Besides the symmetric secondary flows originated behind the rib which is relatively larger in size causing peak Nu on the mid-section of the duct for 30° and 45° rib angles.
- The presence of wake region behind the cylindrical rib causing peak Nu in the middle part of the duct for 15° (Nu/Nu_o = 2.45), 30° (Nu/Nu_o = 2.6) and 45° (Nu = 2.57) rib angles. The enhanced turbulence associated with decreased mean velocity along the span wise direction increases the normalized Nu at each z/B location towards channel center line and reaches maximum for the rib angles between 15° and 60°.
- The position of wake region is highly dependent on separation point over the circular rib as wake moves away radially from the axis of the duct for rib angles of 60°, 75° and 90°. The flow deceleration is relatively higher for 60° and 75° rib arrangements resulting in intense wake region. The turbulent flow structures in large scale originates from side wall have marked effect on the heat transfer for the rib angles of 60°, 75° and 90° and with nearly with equal intensity for 15°, 30° and 45°.
- The thermal hydraulic performance factor relatively higher for 60° rib angle at lower Re = 12000 and it marginally increases with increase in Re for 15° rib angle.
- The exergy analysis reveals that the exergy loss is relatively higher for 60° and 75° rib angles for Re = 12000 and the variation is marginal among the rib positions at lower

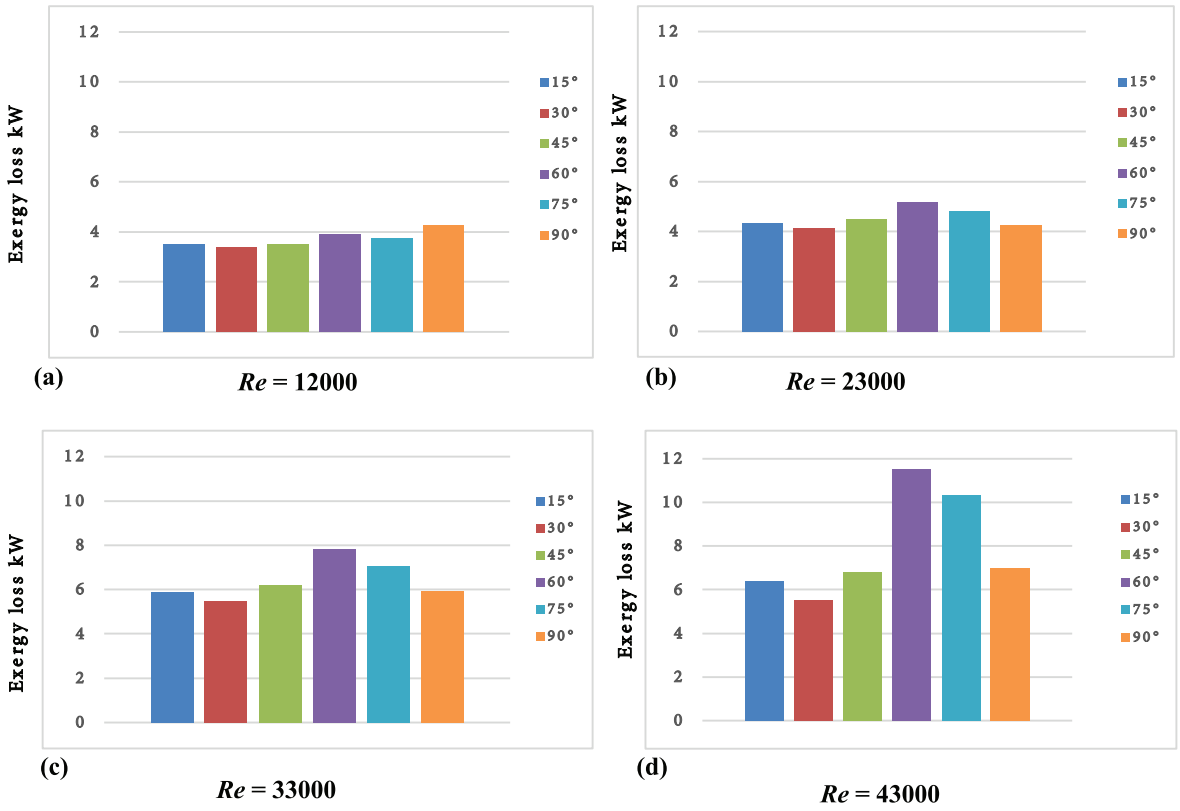

Figure 16. Exergy loss for rib angles of 15° - 90° at *Re* = 12000- 43000.

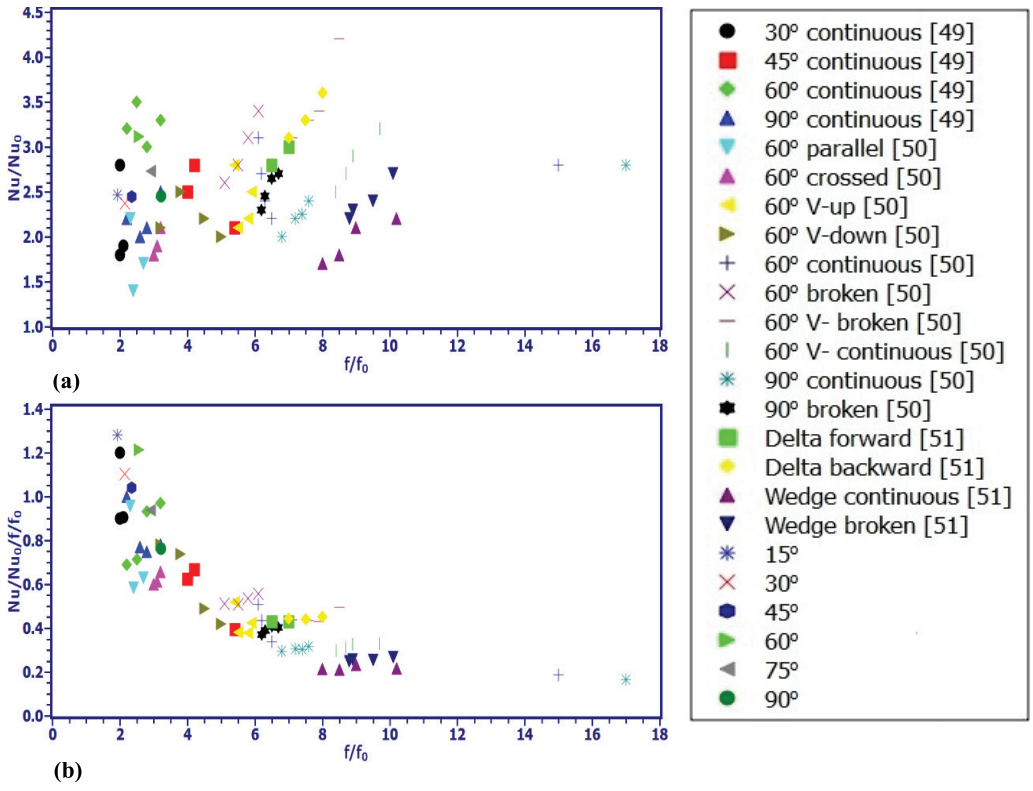

Figure 17. Thermal performance of rib angle of all cases with comparision of results obtained in previous studies (a) Nu/Nu_o as dependendent upon f/f_o (b) $Nu/Nu_o/f/f_o$ as dependent upon f/f_o.

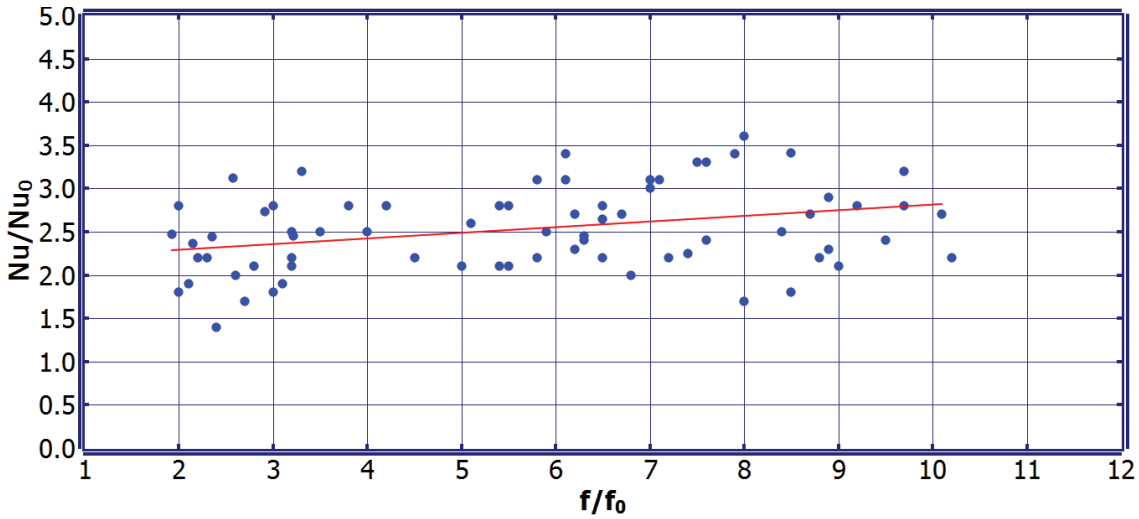

Figure 18. Scatter plot showing the deviation of *Nu/Nuo* as dependent upon f/f_o.

Re. The increase in exergy loss for the 60° and 75° angles is 51.3% and 46.1% respectively when the Re is increased from 23000 to 33000 and it is 47.1% and 45.6% respectively when it is increased from 33000 to 43000.

Some recommendations for future research work are as follows,

- The present numerical study on heat transfer and flow can be further extended for rotating channel with varying heat input.
- The numerical analysis can be carried out for understanding flow physics of two pass channel featuring truncated and circular ribs.
- Experimental optimization is required to find the geometric parameters of the ribs leading to enhanced thermal hydraulic performance

NOMENCLATURE

B	Width of the duct , m
D_h	Hydraulic Diameter, m
d	Diameter of circular rib, m
H	Height of the duct, m
h	Height of the rectangular rib, m
l	Length of the rectangular rib, m
$\dot{E}$	Exergy rate, kW
f	friction factor
f_0	friction factor for a smooth duct
k_a	Thermal conductivity of air, W/m K
L	Length of the duct, m
Nu	Nusselt number
Nu_0	Nusselt number for a smooth duct
ΔP	Pressure drop, N/m^2
p	pitch distance, m
Q	Heat transfer, kW
q	Heat flux, W/m^2
Re	Reynolds number
T_a	Temperature of air, K
T_w	Temperature of wall, K
U	Velocity, m/s
ρ_a	Density of air, kg/m3
ω	Vorticity, s^{-1}

ACKNOWLEDGEMENT

The authors would like to gratefully acknowledge the support provided by B S Abdur Rahman Crescent Institute of Science and Technology during the course of this research.

AUTHORSHIP CONTRIBUTIONS

Conceptualization, Methodology, Resources, Formal analysis and investigation – S.Mohamed Illyas, V.Kumaresan and A. Muthu Manokar. Writing, review and editing – S.Mohamed Illyas, V.Kumaresan and A. Muthu Manokar.

DATA AVAILABILITY STATEMENT

The authors confirm that the data that supports the findings of this study are available within the article. Raw data that support the finding of this study are available from the corresponding author, upon reasonable request.

CONFLICT OF INTEREST

The author declared no potential conflicts of interest with respect to the research, authorship, and/or publication of this article.

ETHICS

There are no ethical issues with the publication of this manuscript.

REFERENCES

[1] Chandra PR, Alexander CR, Han JC. Heat transfer and friction behaviors in rectangular channels with varying number of ribbed wall. Int J Heat Mass Transf 2003;46:481−495. [CrossRef]

[2] Gao X, Sunden B. PIV measurement of the flow field in rectangular ducts with 60° parallel, crossed and V-shaped ribs. Exp Therm Fluid Sci 2004;28:639−653. [CrossRef]

[3] Lu B, Jiang PX. Experimental and numerical investigation of convection heat transfer in a rectangular channel with angled ribs. Exp Therm Fluid Sci 2006;30:513-521. [CrossRef]

[4] Chang SW, Liou TM, Chiang KF, Hong GF. Heat transfer and pressure drop in rectangular channel with compound roughness of V-shaped ribs and deepened scales. Int J Heat Mass Transfer 2008;51:457-468. [CrossRef]

[5] Choudhury R, Das UJ. Viscoelastic effects on the three- Dimensional hydrodynamic flow past a vertical porous plate. Int J Heat and Tech 2013; 31:1-8.

[6] Choi EY, Choi YD, Lee WS, Chung JT, Kwak JS. Heat transfer augmentation using a rib-dimple compound cooling technique. Appl Therma Eng 2013;51:435-441. [CrossRef]

[7] Mohammed H, Al-Aswadi A, Abu-Mulaweh H, Hussein AK, Kanna P. Mixed convection over a backward-facing step in a vertical duct using nanofluids-buoyancy opposing case. J Comp Theor Nanosci 2014;11:1−13. [CrossRef]

[8] Xie G, Liu J, Ligrani PM, Sunden B. Flow structure and heat transfer in a square passage with offset mid-truncated ribs. Int J Heat Mass Transf 2014;71:44-56. [CrossRef]

[9] Yaghmourali Y V, Ahmadi N, Abbaspour-sani E. A thermal-calorimetric gas flow meter with improved isolating feature. Microsyst Technol 2017;23:1927-1936. [CrossRef]

[10] Singh P, Ji Y, Ekkad SV. Experimental and numerical investigation of heat and fluid flow in a square duct featuring criss-cross rib patterns. Appl Therm Eng 2018;128: 415−425. [CrossRef]

[11] Wang L, Wang S, Wen F, Zhou X, Wang Z. Effects of continuous wavy ribs on heat transfer and cooling air flow in a square single-pass channel of turbine blade. Int J Heat Mass Transf 2018;121:514-533. [CrossRef]

[12] Gourari S, Mebarek-Oudina F, Hussein AK, Kolsi L, Hassen W, Younis O. Numerical study of natural convection between two coaxial inclined cylinders. Int J Heat Technol 2019;37:779−786. [CrossRef]

[13] Elkhazen M, Hassen W, Gannoun R, Hussein AK, Borjini M. Numerical study of electro convection in a dielectric layer between two cofocal elliptical cylinders subjected to unipolar injection. J Eng Phys Thermophys 2019;92:1318−1329. [CrossRef]

[14] Laouira H, Oudina F, Hussein AK, Kolsi L, Merah A,Younis O. Heat transfer inside a horizontal channel with an open trapezoidal enclosure subjected to a heat source of different lengths. Heat Transf 2020;49:406−423. [CrossRef]

[15] Ismael M, Hussein AK, Oudina F, Kolsi L. Effect of driven sidewalls on mixed convection in an open trapezoidal cavity with a channel. J Heat Transf 2020;142:082601 [CrossRef]

[16] Bahiraei M, Mazaheri N, Daneshyar MR. CFD analysis of second law characteristics for flow of a hybrid biological nanofluid under rotary motion of a twisted tape: Exergy destruction and entropy generation analyses. Powder Technol 2020;372:351−361. [CrossRef]

[17] Bahiraei M, Mazaheri N, H Siavash. Neural network modeling of thermo-hydraulic attributes and entropy generation of an ecofriendly nanofluid flow inside tubes equipped with novel rotary coaxial double-twisted tape. Powder Technol 2020;369:162−175. [CrossRef]

[18] Jinga Q, Xieb Y, Zhanga D. Numerical investigation of flow and heat transfer in rotating trapezoidal channel with lateral slots and dimple structure. Int Commun Heat Mass Transf 2020;118:104865. [CrossRef]

[19] Pourpasha H, Heris SZ, Mahian O, Wongwises S. The effect of multi-wall carbon nanotubes/turbine meter oil nanofluid concentration on the thermophysical properties of lubricants. Powder Technol 2020;367:133−142. [CrossRef]

[20] Pourpasha H, Farshad P, Heris SZ. Modeling and optimization the effective parameters of nanofluid heat transfer performance using artificial neural network and genetic algorithm method. Energy Rep 2021;7:8447-8464. [CrossRef]

[21] Pourpasha H, Heris SZ, Mohammadfam Y. Comparison between multi-walled carbon nanotubes and titanium dioxide nanoparticles as additives on performance of turbine meter oil nano lubricant. Sci Rep 2021;11:11064. [CrossRef]

[22] Bahiraei M, Mazaheri N. Using spiral channels for intensification of cooling process in an innovative liquid block operated with a biologically produced nanofluid: First and second law analyses. Chem Eng Process 2021;162:108326. [CrossRef]

[23] Lee CS, Shih T P. Effects of heat loads on flow and heat transfer in the entrance region of a cooling duct with a staggered array of pin fins. Int J Heat Mass Transf 2021;175:121302. [CrossRef]

[24] Wei D, Lei L, Yinghou J, Songtao W, Xingchen L, Sunden B. Heat transfer in the trailing region of gas turbines - A state-of-the-art review. Appl Therm Eng 2021;199:117614. [CrossRef]

[25] Luo L, Zhao Z, Qiu D, Wang S , Wang Z, Sunden B. An experimental investigation on the thermal

augmentation of internal endwall in a two-pass duct using an array of delta-winglet vortex generator pair. Int J Heat Mass Transf 2021;182:122043. [CrossRef]
[26] Kumar R, Verma SK. Exergetic and energetic evaluation of an innovative solar air heating system coated with graphene and copper oxide nanoparticles. J Therm Eng 2021;7:447−467. [CrossRef]
[27] Kumar R, Verma SK, Mishra SK, Sharma A, Yadav AS, Sharma N. Performance enhancement of solar air heater using graphene/cerium oxide and graphene-black paint coating on roughened absorber plate. Int J Veh Struct Systems 2022;14:273−279. [CrossRef]
[28] Kumar R, Verma SK. Performance estimation of Triangular Solar air heater roughened absorber surface: An experimental and simulation modeling. Sust Energ Technol Assess 2022;52:102208. [CrossRef]
[29] Bahiraei M, Mazaheri N, Hanooni M. Employing a novel crimped-spiral rib inside a triple-tube heat exchanger working with a nanofluid for solar thermal applications: Irreversibility characteristics. Sust Energ Technol Assess 2022;52:102080. [CrossRef]
[30] Alizadeh H, Pourpasha H, Heris SZ, Estelle P. Experimental investigation on thermal performance of covalently functionalized hydroxylated and non-covalently functionalized multi-walled carbon nanotubes/transformer oil nano fluid. Case Stud Therm Eng 2022;31:101713. [CrossRef]
[31] Soodmand AM, Nejatbakhsh S, Pourpasha H, Aghdasinia H, Heri SZ. Simulation of melting and solidification process of polyethylene glycol 1500 as a PCM in rectangular, triangular, and cylindrical enclosures. Alex Eng J 2022;61:8431−8456. [CrossRef]
[32] Al-Dulaimi MJ, Kareem FA, Hamad FA. Numerical investigation of the heat transfer enhancement inside a square duct with rectangular vortex generators. J Therm Eng 2022;8:1−13. [CrossRef]
[33] Xie G , Zheng S , Zhang W, Sunden B. A numerical study of flow structure and heat transfer in a square channel with ribs combined downstream half-size or same-size ribs. Appl Therm Eng 2013;61:289-300. [CrossRef]
[34] Wang L, Sunden B. Experimental investigation of local heat transfer in a square duct with continuous and truncated ribs. Exp Heat Transf 2005;18:179-197. [CrossRef]
[35] Versteeg HK, Malalasekara W. An Introduction to Computational Fluid Dynamics: The Finite Volume Method. 2nd ed. England: Longman Scientific and Technical Publishers; 1995.
[36] Wang L, Wang S, Wen F, Zhou X, Wang Z. Effects of continuous wavy ribs on heat transfer and cooling air flow in a square single-pass channel of turbine blade. Int J Heat Mass Transf 2018;121:514-533. [CrossRef]
[37] Wongcharee K, Changcharoeny W, Eiamsa ard S. Numerical investigation of flow friction and heat transfer in a channel with various shaped ribs mounted on two opposite ribbed walls. Int J Chem React Eng 2011;9:1−24. [CrossRef]
[38] Liu H, Wang J. Numerical investigation on synthetical performances of fluid flow and heat transfer of semi attached rib-channels. Int J Heat Mass Transf 2011;54:575-583. [CrossRef]
[39] Chaube A, Sahoo PK, Solanki SC. Analysis of heat transfer augmentation and flow characteristics due to rib roughness over absorber plate of a solar air heater. Renew Energ 2006;31:317-331. [CrossRef]
[40] Lin YL, Shih TIP, Stephens MA, Chyu MK. A numerical study of flow and heat transfer in a smooth and ribbed U-duct with and without rotation. J Heat Transf 2001;123:219−232. [CrossRef]
[41] Liu Z, Li J, Feng Z. Numerical study of swirl cooling in a turbine blade leading-edge model. J Thermophys Heat Transf 2015;29:166−178. [CrossRef]
[42] CFX Solver modeling guide Release 14.0 ANSYS, Inc., South pointe, Canonsburg, Pennsylvania, 2011.
[43] Moon MA, Park MJ, Kim KY. Evaluation of heat transfer performances of various rib shapes. Int J Heat Mass Transf 2014;71:275-284. [CrossRef]
[44] Nag P K. Engineering Thermodynamics. 6th ed. India:Tata McGraw Hill; 2017.
[45] Zuckerman N, Lior N. Jet impingement heat transfer: physics, correlations, and numerical modeling. Advan Heat Transf 2006;39:565−631. [CrossRef]
[46] Tanda G. Effect of rib spacing on heat transfer and friction in a rectangular channel with 45° angled rib turbulators on one/two walls. Int J Heat Mass Transf 2011;54:1081−1090. [CrossRef]
[47] Elwekeel FNM, Abdala AMM, Zheng Q. Effects of curved ribs on heat transfer, friction and exergy loss in rectangular cooling channels by CFD. IJST Mech Eng 2021;45:1045-1056. [CrossRef]
[48] Kottayat N, Kumar S, Yadav AK, Anish S. Influence of rectangular ribs on exergetic performance in a triangular duct solar air heater. J Therm Sci Eng Appl 2020;12:051010. [CrossRef]
[49] Han JC, Park JS. Developing heat transfer in rectangular channels with rib turbulators. Int J Heat Mass Transf 1988;31:183-195. [CrossRef]
[50] Han JC, Zhang YM, Lee CP. Augmented heat transfer in square channels with parallel, crossed, and v-shaped angled ribs. J Heat Transf 1991;113:590−596. [CrossRef]
[51] Han JC, Huang JJ, Lee CP. Augmented heat transfer in square channels with wedge-shaped and delta-shaped turbulence promoters. Enhanc Heat Transf 1993;1:37-52. [CrossRef]